Flexible fluorescently labelled colloidal bead chains: synthesis and their real-space studies

Ernest van der Wee

Supervisors:
Dr. Bo Peng
Dr. Hanumantha Rao Vutukuri
Dr. Arnout Imhof
Prof. Dr. Alfons van Blaaderen

June 13, 2013

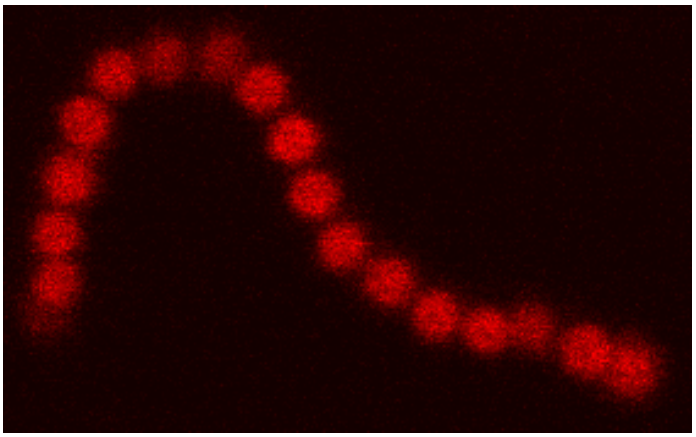

Universiteit Utrecht

Soft Condensed Matter Group
Department of Physics and Astronomy
Faculty of Science
Utrecht University

Contents

Chapter 1

Introduction

1.1 Colloids

Ever since the discovery of the random movement of pollen grains by Robert Brown in 1827 in the highlands of Scotland [1, 2], colloids have been widely researched. Colloids are particles that are small enough to exhibit Brownian motion by undergoing collisions with neighbouring solvent molecules and large enough to be studied by nowadays optical techniques [3]. Examples of colloids are to be found in opals, milk, blood, ink, paint, etc. [4, 5, 6].

The interesting feature of colloids is that they undergo Brownian motion, resulting in phase behaviour similar to that of atoms and molecules [3]. With conventional optical microscopy and confocal laser scanning microscopy [7] the structure and dynamics of colloidal systems can be studied [6, 8, 9, 10]. Additionally, colloids with different morphologies, such as cubes, ellipsoids, rods and disks, as well as different interactions have been studied [11, 12, 13, 14, 15, 16, 17]. By applying external fields (gravity, electric/magnetic fields, shear) on colloidal systems, the phase behaviour of these systems can be manipulated. Next to that, introducing directional, anisotropic interactions using magnetic or electic dipoles lead to anisotropy in systems containing even the most symmetric building blocks: colloidal spheres. Both strategies can be used in the design of advanced materials [18].

1.2 Colloids under electric fields

When colloids are exposed to alternating current (AC) electric fields in a solvent which has a significantly different dielectric constant, induced dipole moments are acquired by the particles. This causes the formation of chain-like aggregates along the direction of the electric field, resulting in a dramatic change of the macroscopic properties of the dispersion (electro-rheological effect). For instance, the viscosity can increase by several orders of magnitude. This feature is being used in industrial applications such as hydraulic valves and displays [3, 19].

During studies on electro-rheological fluids made out of colloids, different structures have been found. For small volume fractions strings of particles along the direction of the electric field have been found [3, 19, 20, 21, 22]. At higher volume fractions with increasing field strength, 2D sheets and crystal

structures were found [3, 20, 23]. These interactions are reversible: when the field is turned off, the particles disperse again into the solution.

Recently, however, a simple method was introduced to bind colloids permanently in a string produced by the application of an AC electric field. Strings of polymer colloids in polar solvents were shortly heated using a hairdryer, yielding permanent strings with varying stiffness [21, 22]. Just as colloids have a similar phase behaviour as atoms and molecules, these permanent strings behave similar to polymer molecules. This makes them suitable as a model system for expanding the theoretical knowledge on polymers and they are expected to assemble into new colloidal structures.

1.3 Research objective

In this research we quantified the flexibility of the colloidal string in the following way. We first synthesized fluorescently labelled PMMA particles in a polar environment and transferred them into different solvents with the optional help of surfactants as in [22, 24, 25]. To be able to study the colloids in the best way possible with confocal laser scanning microscopy, the target solvents had a similar refractive index as the PMMA particles. We investigated a range of solvents to find the one that yielded the best results. The resulting dispersions were exposed to high frequency AC electric fields to align the particles along the direction of the field. After the formation of strings of particles in the system, we followed a simple in-situ thermal annealing step as mentioned in reference [21]. Finally, we analyzed the obtained permanent strings with feature finding and tracking software quantitatively in not only 2D, but also qualitatively in 3D. From the 2D data we measured the thermal shape fluctuations of the chain and thus quantified its flexibility.

Chapter 2

Theory

2.1 Dispersion polymerization

Dispersion polymerization is a commonly used method for the synthesis of micron sized monodisperse colloids. In this single batch process, the polymer colloids precipitate out of a monomer solution, initiated by the decomposition of an initiator. The required components for this reaction are the following:

- Solvent
- Monomer
- Stabilizer (polymer)
- Initiator.

The solvent of choice has to be a good solvent for the monomer, stabilizer and initiator. The resulting polymer, however, should be non-soluble in the solvent. Next to that, the stabilizing polymer (which keeps the polymer particles suspended as a stable colloid) needs to have a higher affinity towards the polymer surface than the solvent [26, 27].

When all ingredients are mixed into a homogeneous solution, the reaction mixture is heated (see fig. 2.1a). This induces the decomposition of the initiator into radicals, which leads to the formation of small oligomers of the monomer (see fig. 2.1b). Once the molecular weight of an oligomer exceeds a certain critical value, the oligomer precipitates from the solution and coagulates with other oligomers (see fig. 2.1c). This goes on until the oligomers are prevented from coagulation through steric stabilization by the stabilizing polymer (see fig. 2.1d). From then on, no new particles are formed and the existing particles grow further by coagulation with oligomers and nuclei and by the polymerization of monomers from the continuous phase (see fig. 2.1e) [26, 27].

2.2 Diffusion of colloids

Due to their relatively small size, colloids are sensitive to their collisions with surrounding solvent molecules. Fluctuations on a small timescale in this process cause the colloids to undergo a “drunkard’s” walk or Brownian motion. The

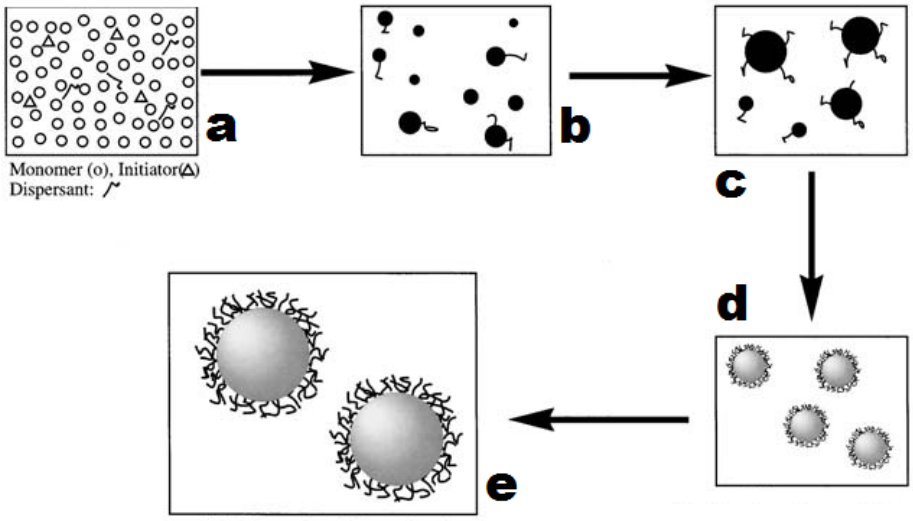

Figure 2.1: *Schematic model of the dispersion polymerization of polymer colloids [27].*

mean squared displacement $< R^2 >$ of a colloidal particle over time (t) can be described as [6]:

$$< R^2 >= n2Dt \tag{2.1}$$

where n is the number of dimensions and D the diffusion coefficient. For the 2D-case we get:

$$< R^2 >= 4Dt \tag{2.2}$$

The diffusion coefficient for a single particle depends on the radius of the particle (r) and the viscosity of the surrounding medium (η), as follows [6]:

$$D = \frac{k_B T}{6\pi\eta r} \tag{2.3}$$

where k_B is the Boltzmann constant and T is the absolute temperature. Note that these equations hold for single particles at very low concentrations. When particles interact with neighbouring particles, their dynamics will be slowed down, resulting in a smaller diffusion coefficient.

2.3 Particle interactions

When our sterically stabilized and charged colloidal particles are dispersed in a solvent with an equal refractive index [8], the Van der Waals forces can be neglected and the interaction potential between the particles can be approximated

with the Yukawa pair-potential as described in [3]:

$$\begin{aligned} \frac{u_{Yukawa}(r_{ij})}{k_B T} &= \begin{cases} \phi \dfrac{exp[-\kappa(r_{ij}-\sigma)]}{r_{ij}/\sigma} & r_{ij} \geq \sigma \\ \infty & r_{ij} < \sigma \end{cases} \\ \text{where} \qquad \phi &= \frac{Z^2}{(1+\kappa\sigma/2)^2} \frac{\lambda_B}{\sigma} \quad , \\ \kappa &= \sqrt{8\pi\lambda_B c} \quad , \\ \text{and} \qquad \lambda_B &= \frac{e^2}{4\pi\epsilon_0\epsilon_m k_B T} \end{aligned} \tag{2.4}$$

where r_{ij} is the center-to-center separation of two particles, k_B the Boltzmann's constant, T the absolute temperature, σ the particle diameter, Z the particle charge, c the monovalent salt concentration, e the elementary charge, ϵ_0 the permittivity of vacuum and ϵ_m the dielectric constant of the solvent. At contact, $r_{ij} = \sigma$ the potential becomes equal to ϕ. The addition of salt to the solvent causes the Debye screening length κ^{-1} to decrease, lowering the potential between to particles and allowing them to get closer.

When the colloidal particles are dispersed in a solvent with a significantly different dielectric constant compared to the particles and an external AC electric field is applied, the particles acquire a dipole moment. The induced dipolar interactions between the particles can be calculated with the point-dipole approximation [28]:

$$\begin{aligned} \frac{u_{dipole}(r_{ij})}{k_B T} &= \frac{\gamma}{2}\left(\frac{\sigma}{r_{ij}}\right)^3 (1 - 3\cos^2\theta_{ij}) \\ \text{where} \qquad \gamma &= \frac{p^2}{2\pi\epsilon_m\epsilon_0\sigma^3 k_B T} \quad , \\ p &= \tfrac{\pi}{2}\beta\epsilon_m\epsilon_0\sigma^3 E_{loc} \quad , \\ \beta &= \frac{\epsilon_p - \epsilon_m}{\epsilon_p + 2\epsilon_m} \quad , \\ \text{and} \qquad E_{loc} &= E + E_{dip} \end{aligned} \tag{2.5}$$

where θ_{ij} is the angle $\mathbf{r}_{ij}$ forms with the direction of the electric field (see fig. 2.2), ϵ_p is the dielectric constant of the particles, E the external electric field, E_{dip} the field induced by the dipoles and E_{loc} the local electric field [3]. It is clear that a large difference between ϵ_p and ϵ_m yields a larger dipole moment p, resulting in a stronger interaction of two particles in equal electric fields. From eq. 2.5 follows that for $\theta_{ij} < 54.7°$ the interaction between the particles will be attractive, while for $\theta_{ij} > 54.7°$ the particles will repel each other. This causes the particles to align in strings (see fig. 2.2).

Figure 2.3 shows the phase diagram of soft sphere particles ($\kappa R = 2$) under an alternating electric field. At low field strength (E_{RMS}) strings of particles form with a timescale on the order of a few seconds. At higher field strengths, the average sphere-sphere spacing decreases and the strings of particles grow until the gap between the electrodes is filled. The long range repulsion of the particles stabilizes the strings, preventing the strings from aggregating further to form sheets. When the electric field is switched off, the string-like structures disappear and the particles disperse again [23, 29, 30].

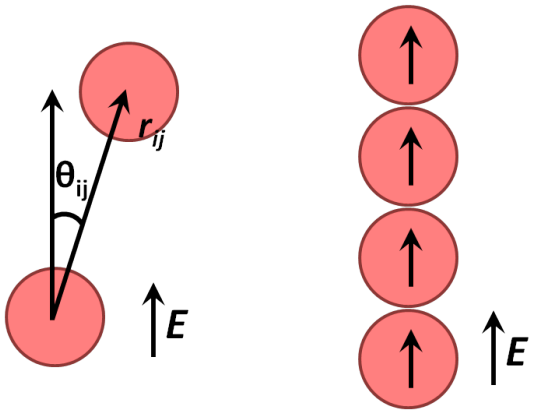

Figure 2.2: *Two particles with the separation vector r_{ij} in an electric field E and their angle θ_{ij} (left) and a string of particles with induced dipole moments aligning in the direction of the electric field (right) [3].*

At even higher field strengths the particles obtain a body-centered tetragonal crystal structure, independent of the volume fraction of the particles in the dispersion.

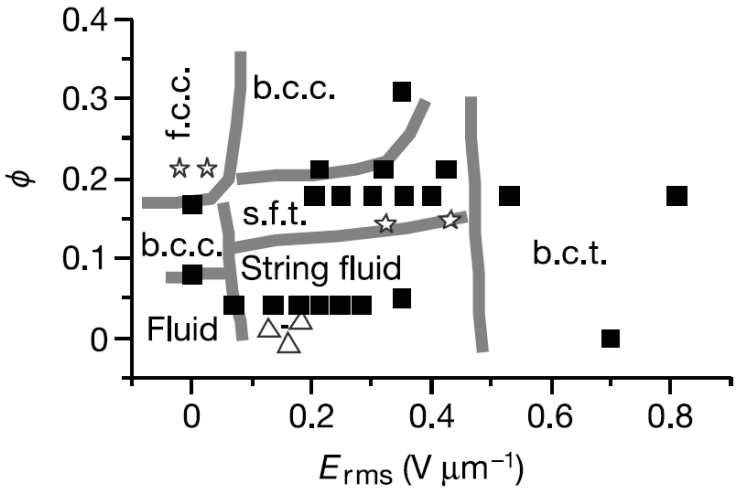

Figure 2.3: *Phase diagram of dipolar soft spheres ($\kappa R = 2$), where E_{RMS} is the electric field strength and ϕ the volume fraction of particles [23].*

2.4 Surfactants

Surfactants, or surface active molecules, are known to lower the interfacial tension between two different phases, such as a polar and apolar liquid [31]. The molecules are amphiphilic, containing a polar head and an apolar tail. Often, the polarity of the head is caused by a local charge in the molecule, for instance

an anionic sulfate group. However, an alcohol or glycol group can also make the molecule surface active. The latter is known as a nonionic surfactant.

The hydrophilic-lipophilic balance (HLB) is a measure of the hydrophilicity or lipophilicity of a surfactant. Davies suggested a method in 1957 to determine this balance [32, 33]:

$$HLB = 7 + mH_h - nH_l \tag{2.6}$$

where m and n are, respectively, the number of hydrophilic and lipophilic groups in the molecule and H_h and H_l the hydrophilic and lipophilic values of the corresponding groups. Surfactants with different HLB values can be used for different systems (see tab. 2.1). It allows us to select a suitable surfactant to stabilize our hydrophylic colloids in apolar solvents.

HLB range	Use
4-6	Water in oil emulsifier
7-9	Wetting agent
8-18	Oil in water emulsifier
13-15	Detergents
15-18	Solubilizing

Table 2.1: *Different HLB value ranges of surfactants and their corresponding use [34].*

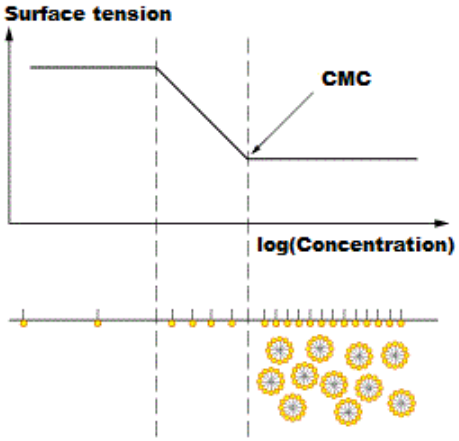

Figure 2.4: *The surface tension versus the surfactant concentration. On addition of the surfactant, the surface tension drops until the critical micelle concentration (CMC) is reached: the surface tension stabilizes [35].*

When a surfactant is added to a system the surface tension changes strongly with the concentration of the surfactant. However, after reaching a certain concentration, the critical micelle concentration (CMC), the surface tension becomes much more stable (see fig. 2.4). This is due to the surfactant molecules forming micelles inside the fluid [36]. When colloids are present in the system, the critical micelle concentration will be higher: the total interface of the system will increase, postponing the formation of micelles to a higher surfactant concentration.

Chapter 3

Methods

3.1 Synthesis of colloidal particles

Our system consisted of sterically stabilized and fluorescently labelled colloids. Two different kind of poly(methyl methacrylate) particles were synthesized by dispersion polymerization in polar solvents as described in [22]. One batch of particles, EPXRII, had a core-shell structure, of which the shell was cross-linked, while the other batch of particles, EPU, had a homogeneous and fully uncross-linked structure.

In the synthesis of particles EPXRII, 31.02 mL methanol, 6.15 g water and 3 g PVP (Polyvinylpyrrolidone K-90 ($\bar{M}_w$ = 360,000 g/mol), Fluka) were mixed. Two-third of this mixture was then put in a 250 mL three-necked roundbottom-flask equipped with a gas supply, a condenser and a Teflon stirring bar. 2.67 mL MM (Methyl methacrylate) and 0.025 g AIBN (Azo-bis-isobutyronitrile, recrystallized from ethanol) were added and the mixture was stirred until it became a homogeneous solution. The system was then bubbled through with nitrogen for half an hour to remove oxygen. After that the flask was heated using a silicone oil bath to 55 ^{o}C and stirred at 100 rpm for 1.5 hours. Next, a mixture of 48.6 μL EGDM (Ethylene glycol dimethacrylate), 2.5 mg RAS dye ((Rhodamine b isothiocyanate)-aminostyrene) and the remaining one-third of the methanol/water/PVP mixture was added during 2 hours at a constant rate of 6.2 mL/h using a peristaltic pump. Finally, 20.5 hours after the complete addition of the mixture, the oil bath was removed to let the reaction mixture cool down to room temperature.

In the synthesis of particles EPU a slightly different procedure was followed: first, 23.26 mL methanol, 2.05 g water and 2 g PVP (Polyvinylpyrrolidone K-90 ($\bar{M}_w$ = 360,000 g/mol), Fluka) were mixed. This mixture was then put in a 250 mL three-necked roundbottom flask equipped with a gas supply, a condenser and a Teflon stirring bar. 2.67 mL MM (Methyl methacrylate) and 0.025 g AIBN (Azo-bis-isobutyronitrile) were added and the mixture was stirred until it became a homogeneous solution. The system was then bubbled through with nitrogen for half an hour to remove oxygen. After that, the flask was heated using a silicone oil bath to 55 ^{o}C and stirred at 100 rpm for 24 hours. Finally, after the 24 hours were past, the oil bath was removed to let the reaction mixture cool down to room temperature.

Both particles were washed several times with methanol to wash away secondary nucleations and other unwanted reaction products. The reaction mixture of particles EPXRII was first centrifuged at 2500 rpm for 135 minutes, after which the supernatant was removed and the dispersion was supplemented with methanol and shaken vigorously. This step was repeated twice, first with a centrifugation speed of 2000 rpm for 30 minutes and second with a centrifugation speed of 1500 rpm for 25 minutes. The reaction mixture containing the EPU particles was transferred to a 40 mL bottle and filled up with methanol and shaken. Next, the following procedure was repeated twice: the mixture was centrifuged at 2500 rpm for 10 minutes, after which the supernatant was removed and the dispersion was supplemented with methanol and shaken. The centrifuge used in these washing steps was a Rotina 46S.

The sizes of the particles and their polydispersities were determined by the use of static light scattering (SLS) and scanning electron microscopy. Figure 3.1 shows the SLS-curves of the two different particles EPU and EPXRII, respectively. They are compared with curves calculated for homogeneous spheres [37]. The experimental curves correspond to a particles diameter of 1.82 μm for the EPU particles and 1.12 μm for the EPXRII particles. Both particles have low polydispersities: 6% for the EPU particles and 5% for the EPXRII particles.

However, when we analyze the image of the EPXRII particles recorded by the scanning electron microscope (SEM), we get a similar size of the particle but a slightly higher polydispersity: 8% (see figure 3.2). This higher polydispersity can be explained by the small amount of particles in the SEM picture and the slightly melted state (due to the electron beam) the PMMA particles are in.

To be able to monitor the EPU particles with a confocal microscope, a fluorescent dye was added after the synthesis using the following procedure [22]: first the particles were transferred from methanol to 1-pentanol. Then 7 mL of a 1.5 g/L rhodamine B dye in 1-pentanol solution was added. Next, 10 volumepercent acetone was added after which the mixture was stirred at 200 rpm for 3 days. The mixture was then heated to 50 ^{o}C for 135 minutes. Finally the excess dye was removed by washing the particles with 1-pentanol a few times. Figure 3.3 shows the succesful incorporation of the dye. Also note the core-shell structure of the EPXRII particle and the difference in the size of the particles. The properties of the particles are summed up in table 3.1.

	EPXRII	EPU
size (SLS)	1.12 μm	1.82 μm
size (SEM)	1.18 μm	-
polydisp. (SLS)	5%	6%
polydisp. (SEM)	8%	-
structure	core-shell	homogeneous
dye addition	during synthesis	after synthesis
crosslinked	shell	no

Table 3.1: *Summary of the properties of the two synthesized particles EPXRII and EPU.*

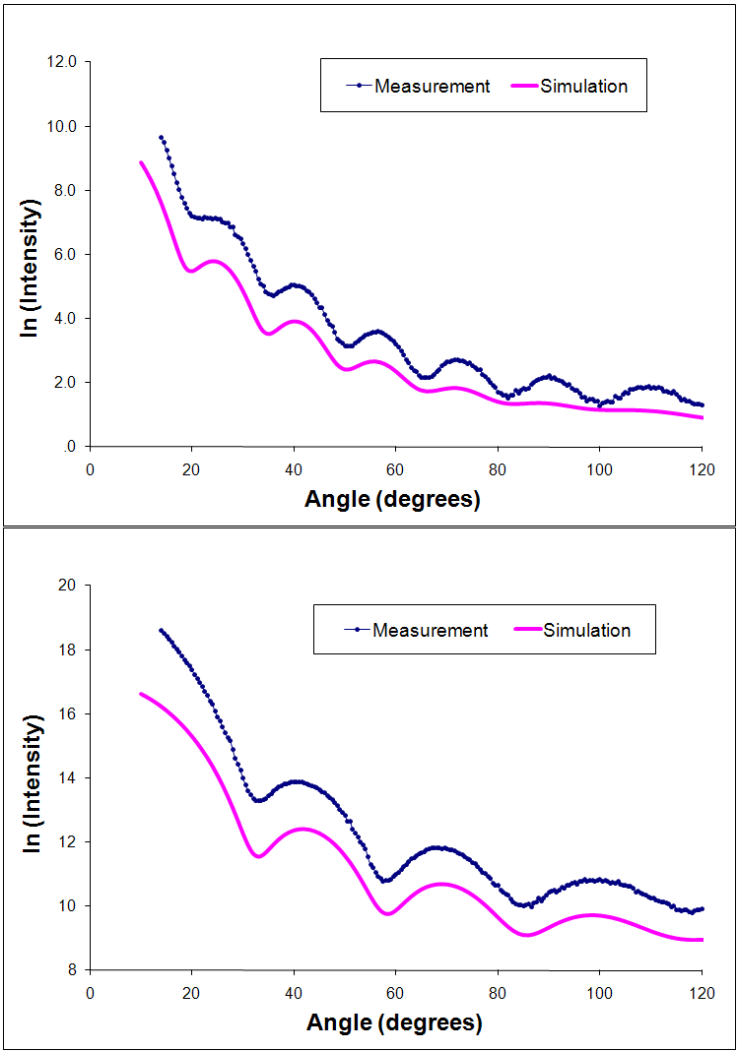

Figure 3.1: *The measured static light scattering curves (blue) with the fitted curves (purple) of the two different particles EPU (top) and EPXRII (bottom). The fitted curves correspond to a particle diameter of 1.82 µm with a polydispersity of 6% for the EPU particles and a particle diameter of 1.12 µm with a polydispersity of 5% for the EPXRII particles. The laser wavelength was 632.8 nm.*

3.2 Studying the colloids

To study the colloids conventional optical microscopy and confocal laser scanning microscopy were used. Samples were prepared by filling a glass capillary (Vitrocom, 0.1 mm x 1 mm) with the dispersion and gluing it on a glass plate with UV-glue (Norland 65). The samples were then exposed to UV radiation for approximately 10-15 minutes with aluminium foil protecting the dispersion. When an electric field was to be applied on the sample, conductive wires (Good-

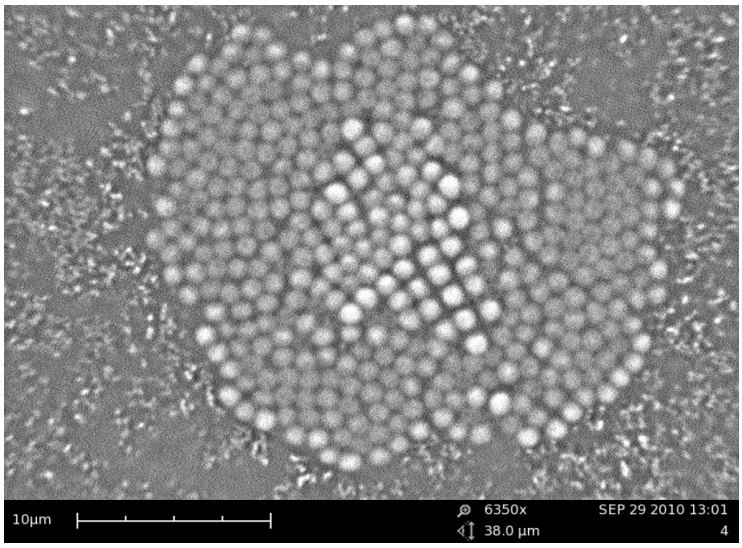

Figure 3.2: *An image of EPXRII particles as recorded by scanning electron microsopy. From analysis of this image we obtained a particle diameter of 1.18 µm and a polydispersity of 8%.*

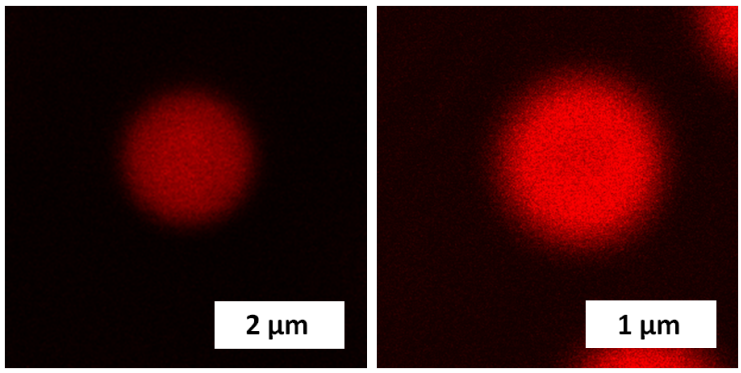

Figure 3.3: *Confocal images of particle EPU (left) and EPXRII (right). The post-synthesis incorporation of the dye made the EPU particles suitable for confocal microscopy.*

fellow, T2 - Thermocouple Alloy Ni95/(Al+Mn+Si)5, ⊘ = 0.025 mm) were placed inside the capillaries along the length direction of the capillary before filling it with the dispersion. In figure 3.4 pictures of the samples can be seen. Because our particles have an opposite charge in respect to the glass walls of the sample cell, they tend to stick to these walls. To prevent the particles from sticking, we coated the cell before use with the polyelectrolyte PVP, the same as used in the particle synthesis (see section 3.1). This coating was applied by dissolving 1 wt% PVP in methanol, which was put into the capillary. Next, the capillary was gently heated in an oven to evaporate the methanol. The capillary was then used as described above.

For optical microscopy a Leica DMRE microscope with a Leica HCX PL

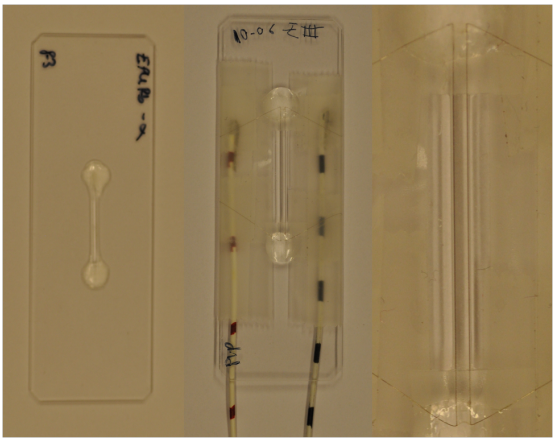

Figure 3.4: *Samples as used for microscopy imaging. Sample without (left) and with conductive wires (middle), and a close-up of the middle picture (right), for a more detailed view on the conductive wires in the capillary.*

Fluotar L 63x/0.70 objective was used. To record images a Nikon photocamera was mounted on the microscope.

For confocal laser scanning microscopy, two different microscopes were used. First a Leica SP2 confocal microscope mounted on an air-pressure stabilized optical table with a 543 nm laser and a 1.40 NA (63×) oil objective with Leica Type F immersion liquid was used. Second, a Nikon C1 confocal microscope mounted on an air-pressure stabilized optical table with 543 nm laser and a 1.32 NA (63×) oil objective with Leica Type F immersion liquid was used.

When an electric field was applied on the samples, an Agilent Technologies 33120A Function generator, 15 MHz was used in combination with a Krohn-Hite 7602M amplifier to apply the electric field. A Tektronix TDS 3012B oscilloscope was used to measure the voltage of the applied field. In all cases an 1 MHz sinusoidal AC field was applied where only the amplitude was varied. A frequency of 1 MHz was chosen since it is high enough to prevent polarization of the electric double layer surrounding the particles [3].

The strings of particles were made permanent by heating the sample with a hair dryer as in [21]. The specific voltages applied to the samples as well as the heating times for every sample are specified in section 4.2.

3.3 Indentification and tracking of particles

For quantative analysis the colloids need to be indentified and tracked in the images of the recorded confocal data. In the case of 2D series of images over time, trajectories of particles were found using the program RyTrack [38]. This program is based on Crocker and Grier's method of particles identification and tracking as can be found on [39] and in [40]. With the help of a script written by R. Besseling the mean squared displacement of the particles was calculated [41]. For the 3D series of images over time, software written in our group by Dr. M. Hermes was used to reconstruct 3D models of the samples over time. The algorithm used was similar to the one that was used in [10].

Chapter 4

Results and discussion

4.1 Transfer of particles to different solvents

To study particles with confocal microscopy, the refractive indices of the particles and the solvent mixture should be equal, this to prevent the laser light of the confocal microscope from scattering inside the sample [42]. To study PMMA particles a solvent mixture of cyclo-hexyl bromide (CHB) and cis-decahydronaphtalene (cis-decalin) with a mass ratio of 2.68 : 1, which is refractive index matched with PMMA, is most commonly used [3, 17, 20]. Furthermore, the density of this mixture is roughly equal to the density of the particles, preventing fast sedimentation. The EPXRII and EPU particles, however, were synthesized in the polar water/methanol mixture. This means aggregation will occur when the particles are dispersed in the apolar CHB/cis-decalin mixture. Therefore it is necessary to transfer the particles with the use of a surfactant to apolar solvents.

The synthesized particles were washed with methanol after their synthesis. However, when the methanol was evaporated, the particles would aggregate irreversibly. Therefore, during the transfer of the particles from one solvent to the other, the particles were washed multiple times with the target solvent. This meant that in the final dispersion traces of the first solvent could still be present.

First, for comparison, EPXRII particles were transferred into different solvents. In the polar solvents tetrahydrofuran (THF) and dimethylsulfoxide (DMSO) the particles dispersed well without the use of a surfactant. In the case of THF, the swelling ratio α ($\alpha = r_S/r_0$, where r_0 is the particle radius in methanol and r_S the radius of the swollen particle as determined from the confocal images) was found to be 1.34, while in DMSO $\alpha = 1.16$ (see fig. 4.1). However, in both cases, the image quality on the confocal microsope degraded. Since the differences between the refractive indices of both solvents and PMMA particles are relatively small (see table 4.1) and therefore the confocal image quality is expected to be good, it is most likely that the solvent somehow quenches the dye, making the particles less visible on the confocal microscope.

When transferring the EPXRII particles into the polar solvent furfuryl alcohol (FFA) the particles were nicely dispersed and the swelling ratio α was found to be 1.61 (see fig. 4.1a). The refractive index of FFA is 1.489, which is almost

PMMA	THF	DMSO	FFA	Formamide
1.491	1.404	1.479	1.489	1.446

Table 4.1: *Refractive indices of PMMA and different polar solvents.*

the same as the refractive index of the particles: 1.491 [43]. Consequently the quality of the confocal images was very good. The core-shell structure of the particles is clearly visible in fig. 4.1a. Additionally another polar solvent with a refractive index close to that of PMMA was used to disperse the particles: formamide has an refractive index of 1.446 [43] and also yields a stable dispersion and good quality confocal images. The swelling ratio α was found to be 1.25 (see fig. 4.1c). Note that both FFA and formamide also have densities, respectively 1.135 g/cm^3 and 1.133 g/cm^3, which are close to the density of PMMA: 1.188 g/cm^3.

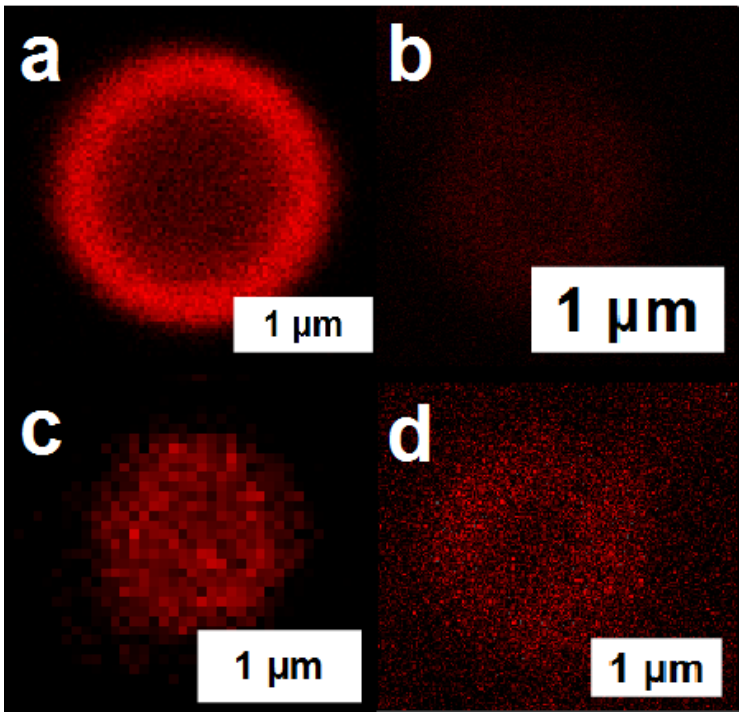

Figure 4.1: *Confocal images of EPXRII particles in different solvents: furfuryl alcohol (a), dimethylsulfoxide (b), formamide (c) and tetrahydrofuran (d).*

In the apolar solvent cyclo-hexyl chloride (CHC) particles could be dispersed, but only if the mass ratio of the wet particles and the total mixture was above ± 0.1. Also, further washing of the particles with CHC would lead to aggregation. This means that probably the methanol, still present after the 'wet' transfer of the particles, prevented the particles from aggregating in CHC. This also explains the aggregation after adding more CHC or additional washing of the particles with CHC, both lowering the methanol concentration. In CHC the particles swelled to a diameter of 1.65 μm, corresponding to a swelling ratio of

1.47.

In the attempts to transfer the particles to different apolar media, different nonionic surfactants were used (see table 4.2). The first one, Lutensol© TO 7, was used to transfer the particles into cyclo-hexyl chloride (CHC). Although at first the particles seem to disperse nicely, after a day the particles aggregated (see fig. 4.3).

Surfactant	HLB-value [25, 33, 44]	Solvent used	Result
Lutensol© TO 7	ca. 12	CHC	unstable
Brij© 30	9	CHC	bad image quality
Span™ 85	1.8	hexane	partly aggregated
		CHB	partly aggregated

Table 4.2: *A list of different surfactants used and their correspondings HLB value, solvent and result.*

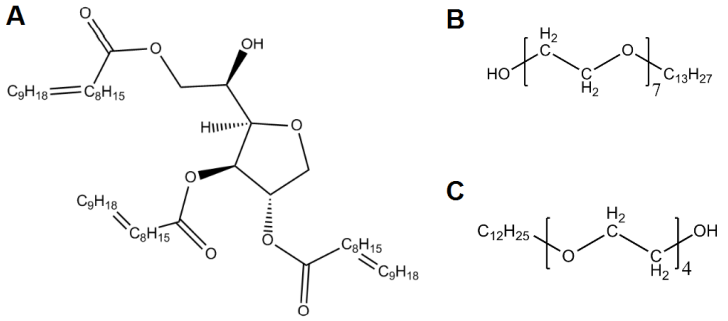

Figure 4.2: *Chemical structures of the surfactants in table 4.2: Span™ 85 (A), Lutensol© TO 7 (B) and Brij© 30 (C).*

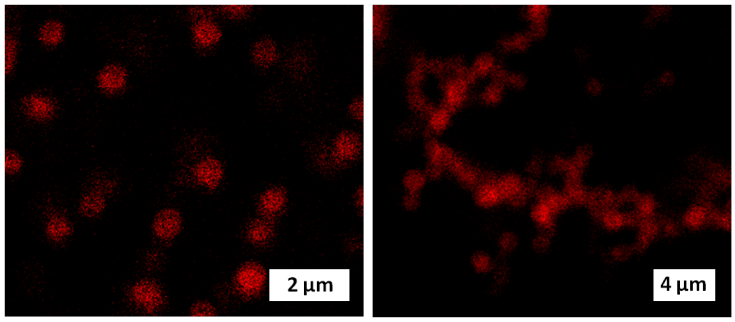

Figure 4.3: *Confocal images of EPXRII particles in CHC with Lutensol© TO 7 surfactant a few hours (left) and a day (right) after transferring.*

Brij© 30 (Sigma) was used in combination with the solvent CHC. Although the particles dispersed nicely, the image quality on the confocal microscope degraded significantly (fig. 4.4), making it impossible to look deep into the sample. This made the surfactant unsuitable for our further experiments.

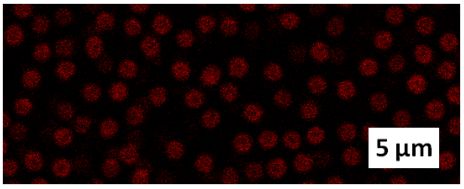

Figure 4.4: *Confocal image of EPXRII particles in CHC with Brij© 30 surfactant, taken in the part of sample that was closest to the microscope objective.*

Behrens *et al.* [25] described how they dispersed commercially bought PMMA-particles (Bangs Laboratories) with a diameter of 0.11, 0.52 and 1.06 μm with the help of the nonionic surfactant Span™ 85 (which has a very low HLB-number (see table 4.2). First they brought the particles from the first solvent, water, into iso-propanol. Next they dissolved Span™ 85 into hexane and transferred the particles into this solution. They found a minimum surfactant concentration of 0.5 mM Span™ 85 for which a stable dispersion of the PMMA particles was obtained.

We tried to disperse our particles in the same way. For the EPU particles a minimum surfactant concentration of 50 mM was needed to prevent severe aggregation of particles. Still, dumbbells and even bigger aggregates were present (see fig. 4.5). When the EPXRII particles were in the same solvent with the same surfactant concentration and a similar particles concentration compared to the EPU particles, more aggregates were present (see fig. 4.5). This can be explained by the higher surface-to-mass ratio of the smaller EPXRII particles compared to the EPU particles. The exact reason for the lower minimum surfactant concentration in [25] is hard to find, due to the fact that they use commercial PMMA particles. The surface properties of those particles might differ from our synthesized particles, resulting in an easier stabilization of their dispersions.

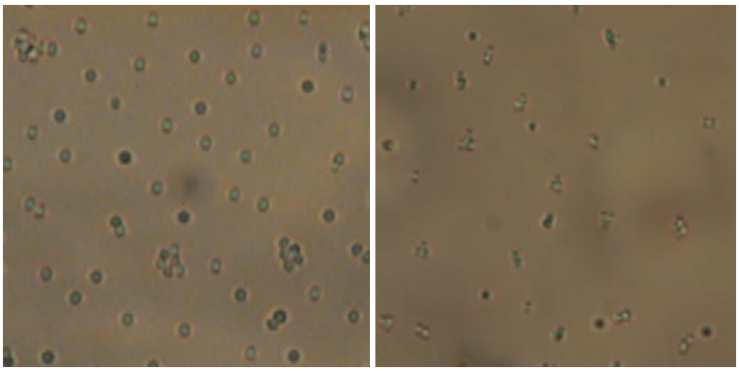

Figure 4.5: *Optical microsope images of EPU (left) and EPXRII (right) particles in hexane with 50 mM Span™ 85. The EPXRII particles appeared to be more clustered than the EPU particles.*

A different method was tried to bring the EPU particles from the polar 1-pentanol to the apolar CHB with the help of Span™ 85. First the particles

were transferred from 1-pentanol into a 100 mM solution of Span™ 85 in hexane. Next CHB was added, with and without Span™ 85 at a concentration of 100 mM, at a ratio (hexane : CHB) of 1:1 and 2:1, yielding 4 different samples. Next the hexane was evaporated by storing the samples without a lid in the fumehood overnight. The properties of the different samples are summarized in table 4.3. To determine the 'quality' of the dispersions, e.g. the percentage of

#	Volume percent CHB in mixture in %	Span™ 85 present in added CHB?	Intermediate Span™ 85 concentration (mM)	Final Span™ 85 concentration (mM)
1	50	yes	100	200
2	33.3	yes	100	300
3	50	no	50	100
4	33.3	no	67	200

Table 4.3: *Properties of samples 1-4. The EPU particles were used in all these samples. The Span™ 85 concentration in hexane was always 100 mM.*

clusters in the dispersions, images were taken of the particles in hexane and the hexane/CHB mixture with an optical microscope (see fig. 4.6). For the particles

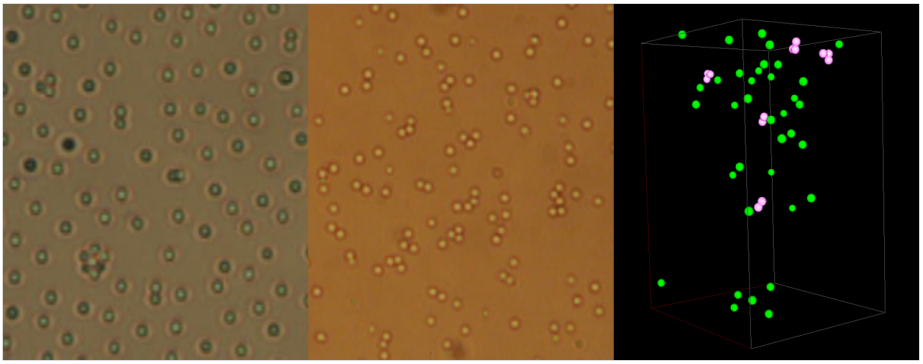

Figure 4.6: *Optical microscope images of the EPU particles in hexane with 100 mM Span™ 85 (left) and hexane/CHB with Span™ 85 (middle) and a 3D data representation of the EPU particles in CHB (right), all from sample 1 (see tab. 4.3). In the 3D representation single particles are colored green while dumbbells or larger clusters are colored pink.*

in CHB, z-stacks were recorded with the confocal microscope and the particles were indentified using the algorithm as described in 3.3. Next the number of clusters, dumbbells and single particles were counted in the images and 3D data sets, in the case of hexane, hexane/CHB and CHB, respectively (see fig. 4.7).

Although the surfactant concentration at different steps in the transfer varies between 50 and 300 mM, the amount of dumbbells and clusters does not change much. This confirms the earlier found minimum Span™ 85 concentration of 50 mM. The quality of the dispersions in CHB are similar to those of the dispersions in hexane, therefore the transfer method seems to be a good way to transfer the particles from hexane to CHB, provided that the intermediate surfactant concentration (in the hexane/CHB mixture) is well above the minimum

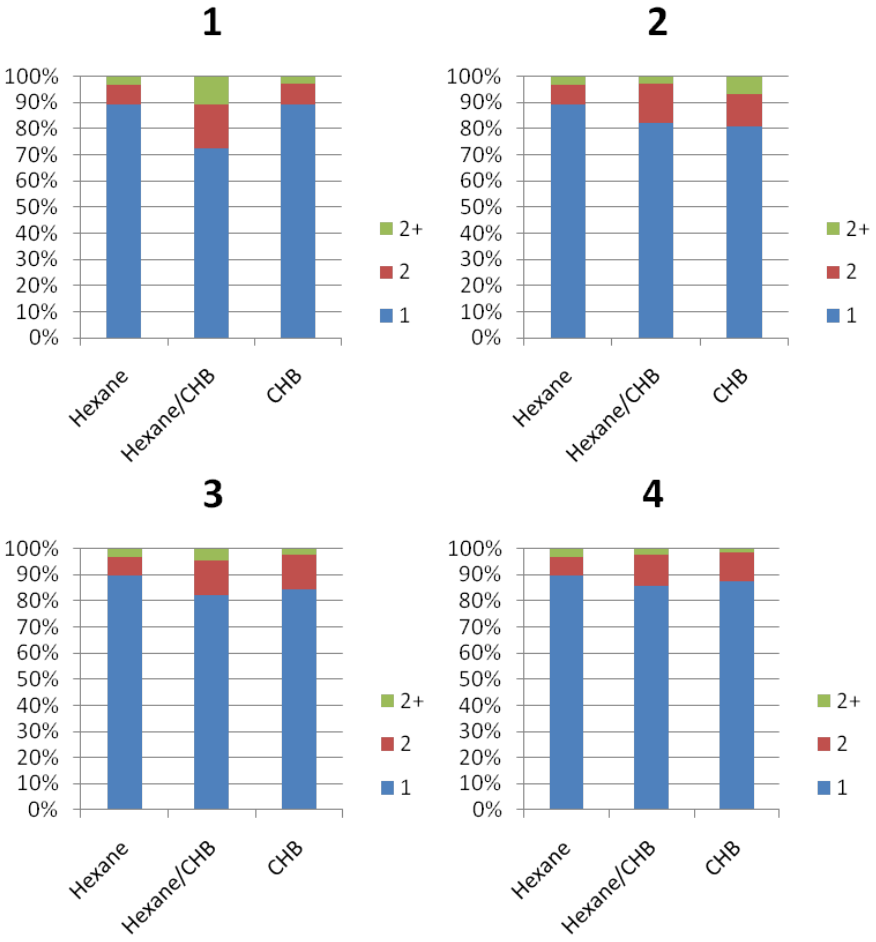

Figure 4.7: *Samples 1-4 and the relative presence of clusters, dumbbells and single particles. Note that in hexane the surfactant concentration is always 100 mM. For the concentrations of surfactant in the hexane/CHB mixture or CHB, for details see table 4.3.*

surfactant concentration for a stable dispersion in CHB. Still, in the best CHB dispersion we got, 20% of the particles were part of a dumbbell or cluster.

4.2 Formation of colloidal strings

As explained earlier in section 2.3, a high frequency AC electric field applied on a dispersion with a large difference in the dielectric constants of the particles and the solvent leads to induced dipole interactions between the particles. AC electric fields were applied on dispersions with different solvents.

First a dispersion of EPXRII particles in CHC without surfactants was used. At a massratio of 0.2 the particles formed aggregates, but when a field of 200

V/mm was applied, loose partices around the aggregates formed strings attached to those aggregates (see fig. 4.8). When the mass ratio was lowered to make

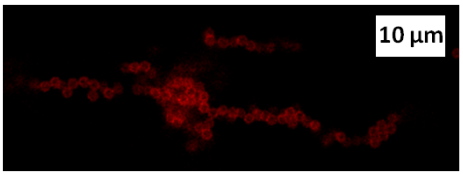

Figure 4.8: *Confocal image of EPXRII particles in CHC under an electric field of 200 V/mm.*

sure the particles would be nicely dispersed, the particles did not respond to the electric field anymore. Since the particles were stored in methanol and could not be dried, transferring the particles was done by centrifuging the dispersion, after which the supernatant was removed. Because the amount of particles was relatively smaller compared to the methanol which could not be removed, the ratio of methanol to particles in the more dilute CHC dispersion was higher. Since the methanol prefers the PMMA particles over the CHC, the presence of methanol slightly increased the dielectric constant of the particle and therefore decreasing the difference between the dielectric constants of the solvent and the particles (see table 4.4). This made the particles less responsive to the alternating electric field.

	PMMA	CHC	Methanol
ϵ_r	2.6	7.6	33

Table 4.4: *Dielectric constants of three different components.*

When samples 1 and 3 from table 4.3, both with EPU particles in CHB with Span™ 85 surfactant, were put in an electric field, strings would form at 200 V/mm. At higher voltages, even up to 800 V/mm, strings grew larger and formed sheets after some time, similar as shown in [3, 20]. After heating the sample with hot air from a hairdryer for 1-2 minutes in order to fix the particles in the strings, the particles were invisible on the confocal microscope. Since the EPU particles were not cross-linked, the high temperature makes them dissolve in CHB, simply destroying the particles.

Additionally, EPXRII particles in furfurylalcohol (FFA) were put in an electric field. Particle strings did form, but at voltages higher than 130 V/mm bubbles appeared in the sample's capillary. After longer exposure to such fields the color of the dispersion went from yellow to brown (see fig. 4.9). These two phenomena imply that the FFA decomposes/reacts after the exposure to a high AC field, therefore the voltage of the field that could be applied without ruining the sample was limited. Attempts at fixing the strings below 130 V/mm failed. To make sure the particles were touching close enough in order to stick together after heating at a lower field strength, the salt lithiumchloride (LiCl) was added to the dispersion. The addition of ions in the dispersion leads to a decrease in the Debye screening length of the particles, allowing them to get closer to another. When a field of 80 V/mm was applied on a dispersion with 0.5M LiCl (reducing the Debye length to approx. 6 nm), short fixed strings were obtained

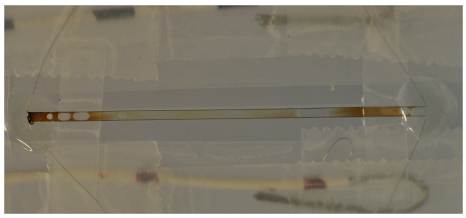

Figure 4.9: *Confocal imaging sample with conductive wires containing a FFA dispersion after applying an electric field of 140 V/mm for 10 hours.*

after the sample had been heated with hot air for 1 minute. These strings consisted of up to 6 particles and were non-flexible. Also, the fixed strings were never straight: they were bended or had a zig-zag pattern (see fig. 4.10). Making

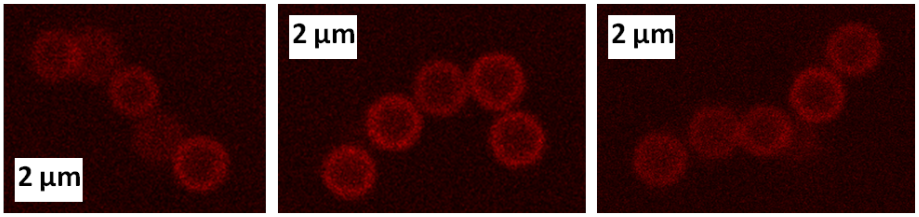

Figure 4.10: *Confocal images of 3 non-flexible strings with different conformations found in a 0.5 M LiCl in FFA sample.*

longer fixed strings in FFA was not possible: a higher voltage or a longer time of heating would result in the decay of the solvent as described earlier. When the electric field was applied for a period in the order of an hour, particles in strings near the capillary wall would stick to the PVP coating. This yielded hexagonal ordered monolayers of colloids with cracks along the direction of the electric field (see fig. 4.11).

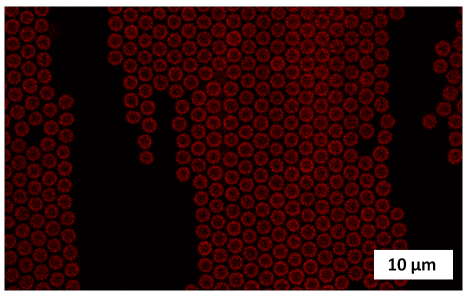

Figure 4.11: *Confocal image of hexagonal ordered monolayers of colloids on the PVP coated wall in a 0.5 M LiCl in FFA sample after exposure to an electric field for an hour.*

Finally, EPXRII particles in formamide were exposed to an electric field. Due to the large difference between the dielectric constant of formamide (ϵ_r = 83) and PMMA (ϵ_r = 2.6) low voltages were sufficient for the formation of

strings. When a field of 50 V_{RMS}/mm was applied for 70 minutes, long strings formed and joined together forming sheets. When the field was slowly turned off, the sheets dissolved and a few very flexible strings with on average six beads remained present (see fig. 4.12). In this method the linking of the particles is

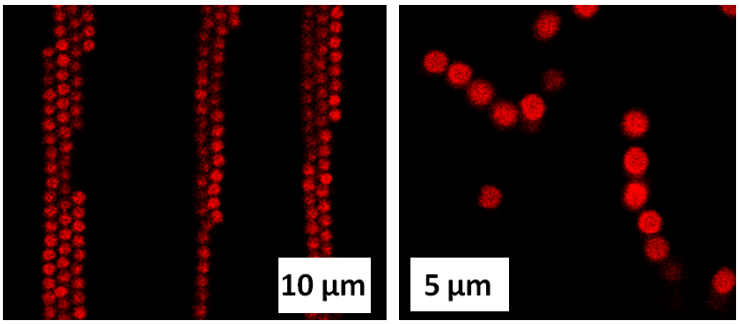

Figure 4.12: *Confocal images of sheets of particles (left) and short strings (right) in the same formamide sample. The sheets formed during an exposure to a 50 V_{RMS}/mm field for 70 minutes. When the field was turned off, the short permanent six bead strings remained.*

achieved without additional heating. This is probably caused by the prolonged exposure to the electric field, which leads to heating the sample itself, making external heating superfluous. The strings, however, are limited in their length and even increasing the voltage to 75 V_{RMS}/mm yielded the same results. The large difference in dielectric constant between the particles and the solvent seems to be required for this self-heating process: when glycerol ($\epsilon_r = 42.5$) was added to the formamide with a mass ratio of 4 : 3 (formamide : glycerol) in order to slow down the dynamics of the particles and lower the density mismatch between the solvent and the particles, much smaller fixed strings were obtained under the same conditions.

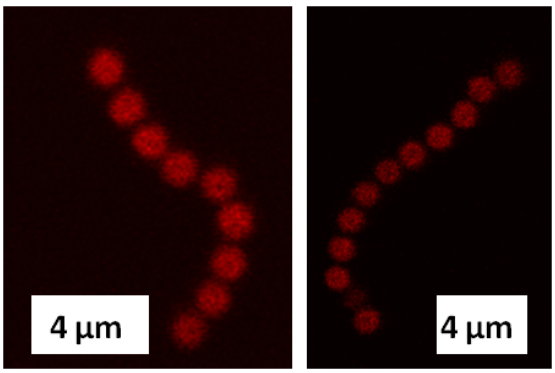

Figure 4.13: *Confocal images of a 9 (left) and 12 (right) bead string in formamide after a 2 hour 75 V_{RMS}/mm electric field and 2 minutes of heating.*

Because of the limited chain length, an electric field of 75 V_{RMS}/mm was applied on a new formamide dispersion sample for 2 hours, allowing the loose particles or small strings enough time to diffuse to the ends of other strings,

resulting in longer chains of particles. Then the sample was heated with hot air from a hairdryer for 2 minutes. Finally, the electric field was turned off slowly after the sample was allowed to cool down for 3 minutes. This yielded long strings with lengths up to 18 beads (see fig. 4.13 and fig. 4.14) which showed much more flexible behaviour compared to the short strings in FFA.

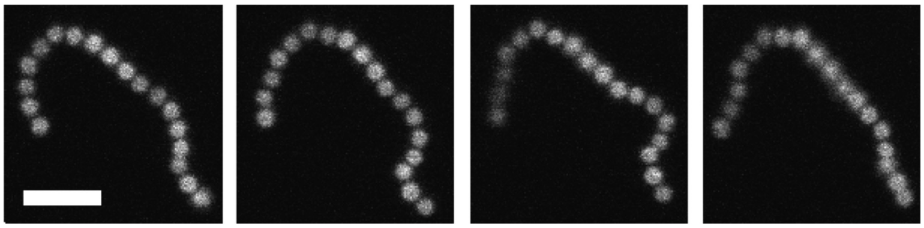

Figure 4.14: *Time-lapse confocal images of the 18 bead string in formamide. The total recording time of the serie of images was 34 seconds. The scale bar is 5 μm.*

4.3 2D analysis of colloidal strings

For a 2D analysis of the permanent strings, series of images were recorded with the confocal microscope. We selected the strings of particles EPXRII made in formamide because of their length and apparent flexible behaviour. The particles in these series were then tracked as described in 3.3. Fig. 4.15 shows the trajectories of the beads inside different strings. During the recording of the confocal image series, the strings lay in a horizontal plane close to the bottom due to gravity. In fig. 4.16 the trajectories of the beads of the 18 bead

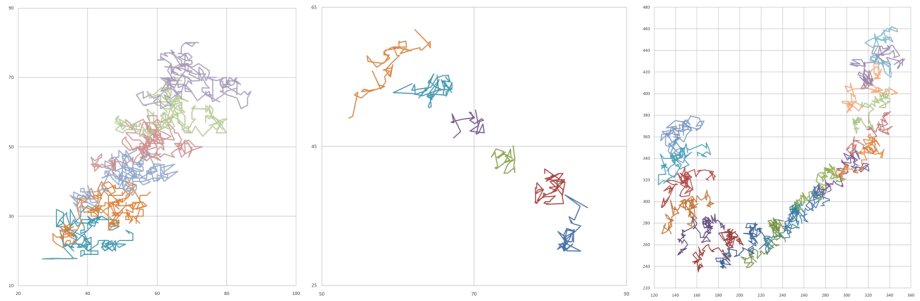

Figure 4.15: *The trajectories of particles inside three differents strings. A six bead string created by exposing a formamide dispersion to 75 V_{RMS}/mm for 75 minutes (left), a six bead string created by exposing a formamide dispersion to 75 V_{RMS}/mm for 30 minutes and heating for one and a half minutes (middle) and an 18 bead string created by exposing a formamide dispersion to 75 V_{RMS}/mm for two hours and heating for two minutes (right). The time between frames was respectively 0.27, 0.14 and 0.34 seconds.*

strings are laid over a superimposed image of all images in the serie. Because

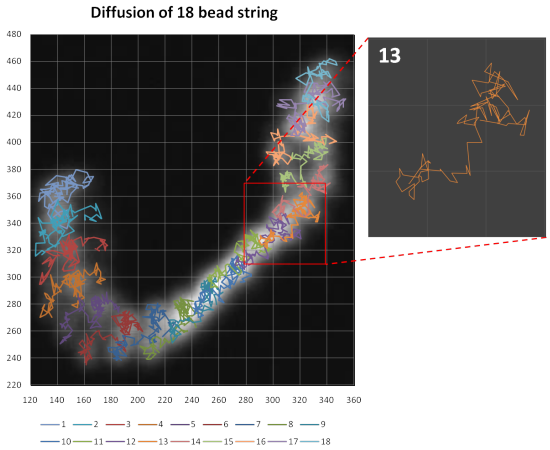

Figure 4.16: *The trajectories of the particles in the 18 bead string laid over the superimposed image of all confocal microscopy images in the serie. The inset shows the trajectory of bead number 13 in the string.*

the trajectories of the beads nicely overlap with the superimposed image the tracking method appears to be reliable.

Since the length of the image series recorded for the smaller strings was limited, only the tracking data of the 18 bead string could be used for the calculation of the mean squared displacement and diffusion constant. For the 18 bead string the mean squared displacement (MSD) of all particles was calculated from the different positions of the beads over time. In fig. 4.17 the MSD was plotted versus the timesteps. The measured curve (red points) becomes linear after $dt = 10$. When fitting a line through this part, the slope will give us the long-time translational diffusion coefficient (D) of all the particles in the string:

$$\begin{aligned} \lim_{t\to\infty} \frac{d}{dt}(<(\Delta x)^2 + (\Delta y)^2>) &= 4D \\ &= 7.4951 \text{ pixels}^2/\text{timestep} \\ D &= 0.0183\ \mu\text{m}^2/\text{sec} \end{aligned}$$

When this value for D is compared to the diffusion coefficient of a single particle in our system, using equation 2.3 (with T = 298 K, $\eta = 3.302 \times 10^{-3}$ Pa·s and r = 0.575×10^{-6} m), we find a value six times as large: 0.115 μm^2/sec, which is expected: unbound particles diffuse more than when they are constrained by bonds to other particles.

From the trajectories of the particles in fig. 4.16 one can see that in all three strings the beads on the end of the strings seem to have more translational freedom compared to the ones in the centre of the string. In fig. 4.17 the mean squared displacement of the particles in the 18 bead string is plotted versus the bead number, showing that the particles on the two tails of the string do indeed move around more.

The bond angles α_i (see fig. 4.18) were calculated for all the bonds ($i = 1 \rightarrow 17$) in the 18 bead string in the whole serie of images, using the formula as in [9]:

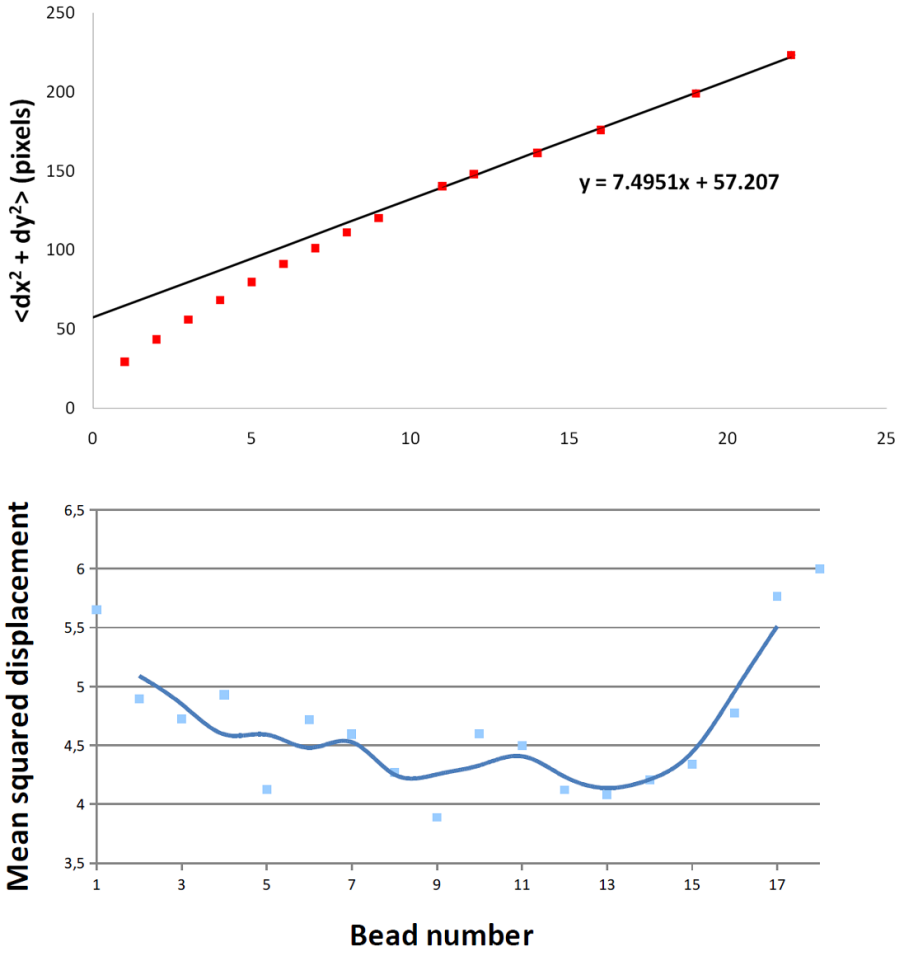

Figure 4.17: *The mean squared displacement of all particles in the string plotted versus timesteps with a linear trendline fitted in the long-time regime (top) and the average displacement of the particles inside the 18 bead string (bottom). The green triangles denote the calculated average displacements, the blue line is the central moving average over three data points.*

$$\begin{aligned} \alpha_i &= j \arccos\left(\frac{\vec{u}_{i+1}\cdot\vec{u}_i}{|\vec{u}_{i+1}||\vec{u}_i|}\right) \\ \text{where} \quad \vec{u}_i &= (x_{n_i} - x_{n_{i-1}}, y_{n_i} - y_{n_{i-1}}) \\ \text{and} \quad j &= \begin{cases} -1 & \text{if} \quad y_i - y_{i-1} > y_{i+1} - y_i \\ +1 & \text{if} \quad y_i - y_{i-1} < y_{i+1} - y_i \end{cases} \end{aligned} \tag{4.1}$$

where j is introduced because the arc-cosine function does not give negative values for negative angles. In fig. 4.18 the distribution of all bond angles is plotted. The bond angles show to have a preference towards a positive value. This matches with fig. 4.16: the 18 bead string is curved in one direction during the recording of the serie of images.

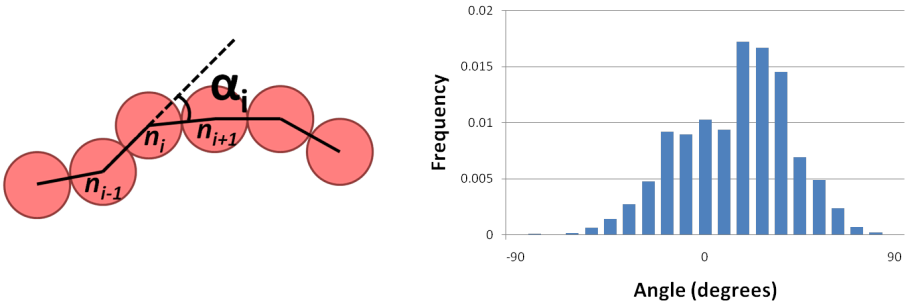

Figure 4.18: *The definition of bond angle α_i (left) and the distribution of all calculated bond angles in the 18 bead string.*

The flexibility of a string of particles can be quantified by the estimation of the persistence length λ_p, the distance over which the local direction of the chain is no longer correlated [45]. It can be approximated in segment lengths from the average cosine of all bond angles [46, 47]:

$$\lambda_p = \frac{1}{1 - \langle \cos(\alpha_i) \rangle}. \tag{4.2}$$

With our calculated bond angles, a persistence length λ_p of 9 segments is approximated for the bead string with a contour length λ_c of 18 segments. Although this found persistence length is expected to be an underestimate [47], the ratio λ_p/λ_c is on the order of one. The flexibility of bead chains can be classified in the following way: when $\lambda_p/\lambda_c \ll 1$ the chains have a flexible nature, when $\lambda_p/\lambda_c \approx 1$ the chains are semiflexible and when $\lambda_p/\lambda_c \gg 1$ the chains are rigid [21]. From this we can conclude that this string of particles is a semiflexible chain. This result is similar to the measurements on a 15 bead polysterene string in DMSO [21].

4.4 3D analysis of colloidal strings

For a 3D study of a colloidal string, a 5 bead string was made by applying a voltage of 50 V_{RMS}/mm for 3 hours and 15 minutes to a dispersion of EPXRII particles in a formamide/glycerol mixture. Next, 63 z-stacks of the string just above the bottom wall were recorded over a total time of 38.7 seconds. The particles in the z-stack were then identified as described in 3.3. 3D reconstructions of the z-stacks are shown in fig. 4.19. Although the movement of the string can be followed in the reconstructions there are some problems.

In order to identify the particles in the z-stack a minimum resolution of 5 pixels per particle in all dimensions is needed. Additionally, the scanning speed of the confocal microscopes used in this research was limited. Therefore, only a small 3D space in the sample could be recorded without having a too large time gap between two consecutive frames. When the gap becomes too large the dynamics of the string cannot be studied in a reliable way. Due to limited size of the 3D frame, a particle in the string sometimes diffuses out of the 3D space

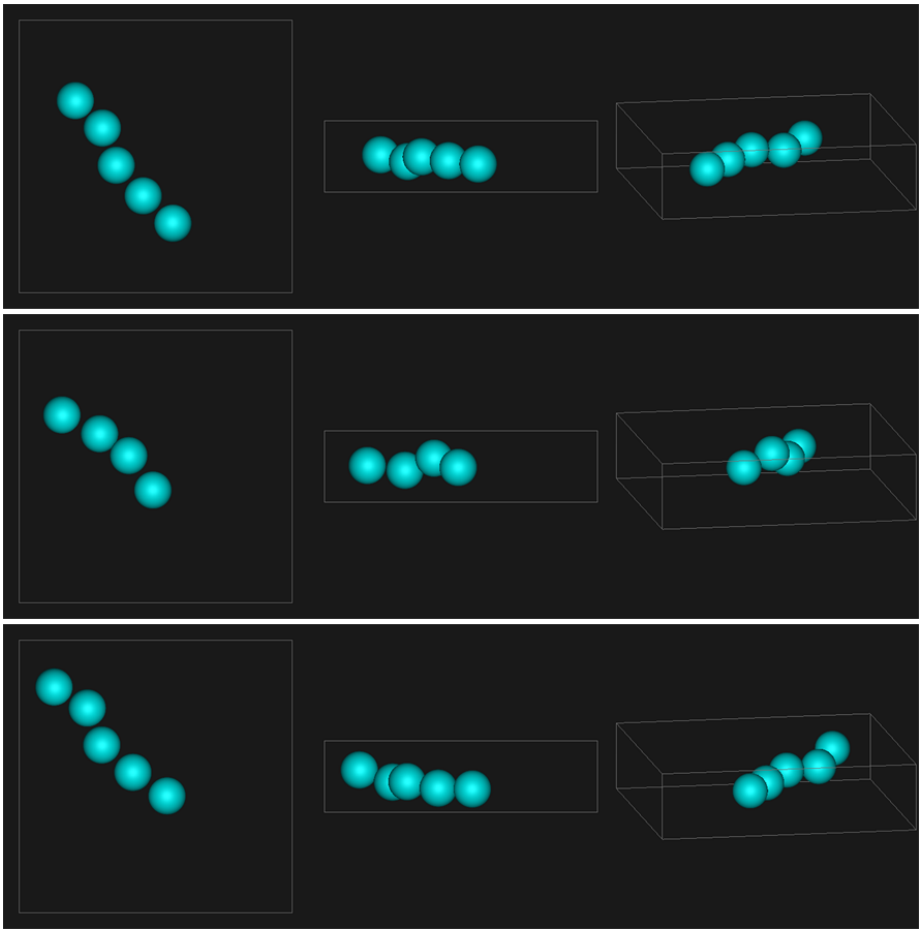

Figure 4.19: *3D reconstruction of a 5 bead string from three different perspectives with framenumber 1 (top), 15 (middle) and 30 (bottom). Note the missing particle in frame 15.*

of the z-stack (see fig. 4.19). This limitation also made it impossible to study a 9 bead string in 3D with the confocal microscope.

Chapter 5

Conclusions and outlook

We succesfully synthesized homogenous and core-shell crosslinked PMMA particles in a polar solvent mixture, which aggregated irreversibly when dried. We transferred these particles to several solvents in order to find one in which the particles could be assembled into flexible strings that could also be imaged with confocal microscopy for the analysis of their dynamics. The particles could be easily dispersed in different polar solvents. With the use of different surfactants we tried to transfer the particles also to apolar solvents. When using Span™ 85 as surfactant the particles were stable in CHC, although 20% of the particles were aggregated and a much higher surfactant concentration was needed than in literature [25]. The latter is probably due to the differences in the surface of the particles used in this work and in literature.

When AC electric fields were applied on the dispersions of particles in CHC, FFA, formamide, a mixture of formamide/glycerol and a mixture of Span™ 85/CHB, strings of particles formed in the dispersions along the direction of the electric field. In FFA with added salt the strings of particles could be made permanent by heating the sample, resulting in stiff strings of max. 6 beads. When in formamide and the formamide/glycerol mixture a field was applied for more than an hour, permanent flexible strings were obtained, which had a length of ± 6 beads. But additional heating even yielded long flexible strings up to 18 beads.

With the help of tracking software, the trajectories of the particles in 2D in some strings were determined. For the 18 bead string we calculated the long-time translational diffusion constant from the mean squared displacement of all the particles in the string, which was, understandably, lower than the translational diffusion constant of a single particle. Additionally, the mean squared displacement of the particles in the string showed that the particles on the ends of the string have more translational freedom than the particles in the centre of the string. The calculated angle distribution of the string corresponded to the configuration of the string. With the calculated bond angles the persistence length of the 18 bead string was estimated to be 9 segments long, which corresponds to a semiflexible nature of the bead chain.

Finally, we recorded 3D data of a 5 bead string over time. But due to the limited scanning frequencies of the used confocal microscopes this data was not good enough to do quantative analysis.

In the future it would be interesting to study even longer strings with con-

focal microscopy. To do so two things could be altered. First, the dynamics of the string can be slowed down by raising the viscosity of the solvent used, using the formamide/glycerol mixture, instead of pure formamide. Second, a confocal microscope with a faster scanning speed will improve the quality of 3D data.

Acknowledgements

I would like to thank Bo and Rao for their guidance and advice in the completion of this work. Next to that I would like to thank Thijs for his advice on the identification and tracking of the particles. Additionally, I would like to thank Arnout and Alfons for the useful discussions and suggestions. Last I would like to thank all the people of the Soft Condensed Matter and Biophysics group for the pleasant working environment.

Bibliography

[1] R. Brown, "A brief account of microscopical observations made in the months of june, july and august, 1827, on the particles contained in the pollen of plants; and on the general existence of active molecules in organic and inorganic bodies.," *Phil. Mag.*, vol. 4, p. 161, 1828.

[2] J. Burnett, *The vegetation of Scotland*. Oliver and Boyd Ltd., 1964.

[3] M. Leunissen, *Manipulating Colloids with Charges & Electric Fields*. PhD thesis, Utrecht University, 2007.

[4] J. V. Sanders, "Colours of precious opal," *Nature*, vol. 204, p. 1151, 1964.

[5] J. V. Sanders, "Close-packed structures of spheres of two different sizes. i. observations on natural opal.," *Philosophical Magazine A*, vol. 42(6), p. 705, 1980.

[6] R. Hunter, *Foundations of colloid science*. Oxford University Press, 2nd ed., 2009.

[7] N. A. M. Verhaegh and A. v. Blaaderen, "Dispersions of rhodamine-labeled silica spheres - synthesis, characterization, and fluorescence confocal scanning laser microscopy," *Langmuir*, vol. 10(5), p. 1427, 1994.

[8] W. Russel, D. Saville, and W. Schowalter, *Colloidal Dispersions*. Cambridge University Press, 1999.

[9] D. Li, N. Fakhri, M. Pasquali, and S. Biswal, "Axial thermal rotation of slender rods," *Physical Review Letters*, vol. 106, p. 188302, 2011.

[10] A. v. Blaaderen and P. Wiltzius, "Real-space structure of colloidal hard-sphere glasses," *Science*, vol. 270, pp. 1177–1179, 1995.

[11] L. Rossi, S. Sacanna, W. T. M. Irvine, P. M. Chaikin, and D. J. Pine, "Cubic crystals from cubic colloids," *Soft Matter*, vol. 7, pp. 4139–4142, 2011.

[12] D. Mukhija and M. J. Solomon, "Translational and rotational dynamics of colloidal rods by direct visualization with confocal microscopy," *Journal of colloid and interface science*, vol. 314, pp. 98–106, 2007.

[13] A. Kuijk, A. v. Blaaderen, and A. Imhof, "Synthesis of monodisperse, rodlike silica colloids with tunable aspect ratio," *Journal of the American Chemical Society*, vol. 133, pp. 2346–2349, 2011.

[14] A. Petukhov, D. v. d. Beek, R. Dullens, I. Dolbnya, G. Vroege, and H. Lekkerkerker, "Observation of a hexatic columnar liquid crystal of polydisperse colloidal disks," *Physical review letters*, vol. 95, 2005.

[15] B. Ruzicka, E. Zaccarelli, L. Zulian, R. Angelini, M. Sztucki, A. Moussad, T. Narayanan, and F. Sciortino, "Observation of empty liquids and equilibrium gels in a colloidal clay," *Nature Materials*, vol. 10, pp. 56–60, 2011.

[16] D. Kraft, R. Ni, F. Smallenburg, M. Hermes, K. Yoon, D. Weitz, A. v. Blaaderen, J. Groenewold, M. Dijkstra, and W. Kegel, "Surface roughness directed self-assembly of patchy particles into colloidal micelles," *Proceedings of the National Academy of Sciences*, vol. 109, p. 10787, 2012.

[17] T. Vissers, *Oppositely Charged Colloids Out of Equilibrium*. PhD thesis, Utrecht University, 2010.

[18] A. v. Blaaderen, "Colloid under external control," *MRS Bulletin*, vol. 29, pp. 85–90, 2004.

[19] A. P. Hynninen, *Phase Behavior of Charged Colloids and the Effect of External Fields*. PhD thesis, Utrecht University, 2005.

[20] M. Leunissen, R. Vutukuri, and A. v. Blaaderen, "Directing colloidal self-assembly with biaxial electric fields," *Advanced Materials*, vol. 21, pp. 3116–3120, 2009.

[21] H. Vutukuri, A. Demirors, B. Peng, P. v. Oostrum, A. Imhof, and A. v. Blaaderen, "Colloidal analogues of charged and uncharged polymer chains with tunable stiffness," *Angewandte Chemie Int. Ed.*, vol. 51, pp. 11249–11253, 2012.

[22] B. Peng, E. v. d. Wee, A. Imhof, and A. v. Blaaderen, "Synthesis of monodisperse, highly cross-linked, fluorescent PMMA particles by dispersion polymerization," *Langmuir*, vol. 28, pp. 6776–6785, 2012.

[23] A. Yethiraj and A. v. Blaaderen, "A colloidal model system with an interaction tunable from hard sphere to soft and dipolar," *Nature*, vol. 421, pp. 513–517, 2003.

[24] B. Peng, H. Vutukuri, A. v. Blaaderen, and A. Imhof, "Synthesis of fluorescent monodisperse non-spherical dumbbell-like model colloids," *Journal of Materials Chemistry*, vol. 22, pp. 21893–21900, 2012.

[25] S. Behrens and et al., "Particle charging and charge screening in nonpolar dispersions with nonionic surfactants," *Langmuir*, vol. 26, pp. 16941–16948, 2010.

[26] R. M. Fitch, *Polymer Colloids: A Comprehensive Introduction*. Academic Press, 1997.

[27] S. Kawaguchi and K. Ito, "Dispersion polymerization," *Advanced Polymer Science*, vol. 175, pp. 299–328, 2005.

[28] J. Jackson, *Classical Electrodynamics*. Wiley, 1999.

[29] A. P. Hynninen and M. Dijkstra, "Phase behaviour of dipolar hard and soft spheres," *Physical Review E*, vol. 72, p. 051402, 2005.

[30] A. P. Hynninen and M. Dijkstra, "Phase diagram of dipolar hard and soft spheres: manipulation of colloidal crystal structures by an external field," *Physical Review Letters*, vol. 94, p. 138303, 2005.

[31] T. Witten and P. Pincus, *Structured fluids: Polymers, Colloids, Surfactants*. Oxford University Press, 2004.

[32] J. Davies, "A quantitative kinetic theory of emulsion type, i. physical chemistry of the emulsifying agent," in *Proceedings of the International Congress of Surface Activity*, pp. 426–438, 1957.

[33] M. Schick, *Nonionic Surfactants: Physical Chemistry*. Marcel Dekker, Inc., 1st ed., 1987.

[34] W. Griffin, "Classification of surface-active agents by HLB," *J. Soc. Cosmet. Chem.*, vol. 1, pp. 311–326, 1949.

[35] J. Kunjappu, "Ink chemistry." `http://www.rsc.org/chemistryworld/Issues/2003/March/inkchemistry.asp`, August 2011.

[36] A. Dominquez, A. Fernandez, N. Gonzalez, E. Iglesias, and L. Montenegro, "Determination of critical micelle concentration of some surfactants by three techniques," *Journal of chemical education*, vol. 74, pp. 1227–1231, 1997.

[37] C. Bohren and D. Huffman, *Absorption and Scattering of Light by Small Particles*. John Wiley & Sons, Inc., 1983.

[38] R. Smith and S. Spaulding, "User friendly, freeware image segmentation and particle tracking." `http://www.iwu.edu/~gspaldin/rytrack.html`, August 2011.

[39] E. Weeks, "Particle tracking using IDL." `http://www.physics.emory.edu/~weeks/idl/`, August 2011.

[40] J. Crocker and D. Grier, "Methods of digital video microscopy for colloidal studies," *Journal of colloid and interface science*, vol. 179, pp. 298–310, 1995.

[41] R. Besseling, "Msd_app.sav." `http://www2.ph.ed.ac.uk/~rbesseli/ITN/msd_app.sav`, August 2011.

[42] A. v. Blaaderen, "Imaging individual particles in concentrated colloidal dispersions by confocal scanning light microscopy," *Advanced Materials*, vol. 5, pp. 52–54, 1993.

[43] J. Brandrup, E. Immergut, and E. Grulke, *Polymer Handbook*. John Wiley & Sons, Inc., 4th ed., 1999.

[44] M. Rabiskova and J. Valaskova, "The influence of HLB on the encapsulation of oils by complex coacervation," *J. Microencapsulation*, vol. 15, pp. 747–751, 1998.

[45] H. R. Vutukuri, *Complex Colloidal Structures by Self-assembly in Electric Fields*. PhD thesis, Utrecht University, 2012.

[46] P. Cifra, "Differences and limits in estimates of persistence length for semi-flexible macromolecules," *Polymer*, vol. 45, pp. 5995–6002, 2004.

[47] P. v. Oostrum, *Using Light Scattering to Track, Characterize and Manipulate Colloids*. PhD thesis, Utrecht University, 2011.